European Journal of Radiology Open 14 (2025) 100630

Contents lists available at ScienceDirect

European Journal of Radiology Open

journal homepage: www.elsevier.com/locate/ejro

# CT-based intratumoral and peritumoral radiomics nomogram to predict spread through air spaces in lung adenocarcinoma with diameter ≤ 3 cm: A multicenter study

Yangfan Su [a,b,1], Junli Tao [a,b,1], Xiaosong Lan [a,b], Changyu Liang [a,b], Xuemei Huang [a,b], Jiuquan Zhang [a,b], Kai Li [c,*], Lihua Chen [a,b,**]

[a] Department of Radiology, Chongqing University Cancer Hospital & Chongqing Cancer Institute & Chongqing Cancer Hospital, No. 181 Hanyu road, Shapingba district, Chongqing 400030, China
[b] Key Laboratory for Biorheological Science and Technology of Ministry of Education (Chongqing University), Chongqing University Cancer Hospital & Chongqing Cancer Institute & Chongqing Cancer Hospital, No. 181 Hanyu road, Shapingba district, Chongqing 400030, China
[c] Department of Radiology, The First Affiliated Hospital of Guangxi Medical University, No. 6 Shuangyong road, Qingxiu district, Nanning, Guangxi Zhuang Autonomous Region 530021, China

## HIGHLIGHTS

- Peritumoral information is important for predicting STAS status.
- The model based on intratumoral and peritumoral information improved performance.
- The radiomics nomogram has a stably and accurately clinical application.

## ARTICLE INFO

*Keywords:*
Lung
Adenocarcinoma
Neoplasm invasiveness
Radiomics
Nomograms

## ABSTRACT

*Purpose:* The aim of this study was to explore and develop a preoperative and noninvasive model for predicting spread through air spaces (STAS) status in lung adenocarcinoma (LUAD) with diameter ≤ 3 cm.
*Methods:* This multicenter retrospective study included 640 LUAD patients. Center I included 525 patients (368 in the training cohort and 157 in the validation cohort); center II included 115 patients (the test cohort). We extracted radiomics features from the intratumor, extended tumor and peritumor regions. Multivariate logistic regression and boruta algorithm were used to select clinical independent risk factors and radiomics features, respectively. We developed a clinical model and four radiomics models (the intratumor model, extended tumor model, peritumor model and fusion model). A nomogram based on prediction probability value of the optimal radiomics model and clinical independent risk factors was developed to predict STAS status.
*Results:* Maximum diameter and nodule type were clinical independent risk factors. The extended tumor model achieved satisfactory STAS status discrimination performance with the AUC of 0.74, 0.71 and 0.80 in the three cohorts, respectively, performed better than other radiomics models. The integrated discrimination improvement value revealed that the nomogram outperformed compared to the clinical model with the value of 12 %. Patients with high nomogram score (≥ 77.31) will be identified as STAS-positive.

*Abbreviations:* AUC, Area under curve; CT, Computed tomography; DCA, Decision curve analysis; ET, Extended tumor; IDI, Integrated discrimination improvement; ICC, Intra-class correlation coefficient; IT, Intratumor; LUAD, Lung adenocarcinoma; PT, Peritumor; ROC, Receiver operating characteristic; ROI, Region of interest; STAS, Spread through air spaces.

* Corresponding author.
** Correspondence to: Department of Radiology, Chongqing University Cancer Hospital, No. 181 Hanyu road, Shapingba district, Chongqing 400030, China.
*E-mail addresses:* taojunli0712@163.com (J. Tao), lcy20100310@163.com (C. Liang), huangxm_00@163.com (X. Huang), doctorlikai@126.com (K. Li), clhaaa2002@163.com (L. Chen).

[1] These authors contributed equally to this work.

https://doi.org/10.1016/j.ejro.2024.100630
Received 14 October 2024; Received in revised form 24 December 2024; Accepted 27 December 2024

*Conclusions:* Peritumoral information is significant to predict STAS status. The nomogram based on the extended tumor model and clinical independent risk factors provided good preoperative prediction of STAS status in LUAD with diameter $\leq 3$ cm, aiding surgical decision-making.

## 1. Introduction

Lung cancer is the leading cause of malignancy-related deaths, which may be related to its unique invasion pattern [1]. In 2015, the World Health Organization (WHO) officially proposed a new invasion pattern of lung cancer, the concept of spread through air spaces (STAS) [2]. Surgery is the primary treatment option for early-stage lung cancer, and selection of the surgical method is mainly based on the size of the tumor. Previous studies have shown that sublobectomy is feasible when the tumor diameter $\leq 3$ cm [3,4]. However, in patients with STAS-positive, sublobectomy would cause higher postoperative recurrence rate and poorer prognosis than lobectomy [5,6]. Therefore, for tumors with diameter $\leq 3$ cm, accurate preoperative prediction of STAS status is particularly important for developing surgical plans and improving prognosis.

At present, the gold standard for STAS diagnosis is postoperative pathological examination, which cannot substantially affect surgical decisions. The accuracy and sensitivity of preoperative bronchoscopic cytology and intraoperative freezing are still limited [7,8]. As a noninvasive examination method, computed tomography (CT) may help predict STAS status preoperatively. Previous studies have shown that some CT morphological features, such as percentage of solid component [9] and absence of ground-glass opacity [10], were closely related to STAS-positive in lung adenocarcinoma (LUAD). However, the evaluation of morphological features heavily relies on the radiologist's subjective interpretation, which inevitably leads to inestimable misdiagnosis and overdiagnosis.

Radiomics is a method of converting images into data, mining and analyzing them to develop a model for clinical decision-making. Automatically extracting radiomics features by computer can avoid errors caused by subjective interpretation [11]. The majority of current studies [12–15] have focused on intratumoral radiomics, may only indirectly predict STAS status. From the biological perspective, as STAS is distributed in the lung parenchyma around the tumor, there may be more valuable information in the peritumoral than in intratumoral area. However, fewer studies pay attention to peritumoral radiomics, the generalization of them is limited by the small sample size [16,17] and lack of external validation [18,19]. Furthermore, overlooked of integrating radiomics with clinical information and lack of risk stratification let lots above-mentioned studies were inaccessible to clinical practice. Therefore, developing a risk stratification model based on large sample of clinical, intratumoral and peritumoral information, and validating it in different centers, is necessary to stably and accurately predict STAT status.

The purpose of this study was to explore the value of intratumoral and peritumoral information in predicting STAS status, and to develop a nomogram based on the optimal radiomics model and clinical independent risk factors to provide decision support for surgery planning in LUAD with diameter $\leq 3$ cm.

## 2. Methods

### 2.1. Patient selection

The study was conducted in accordance with the Declaration of Helsinki (as revised in 2013). This retrospective study was approved by

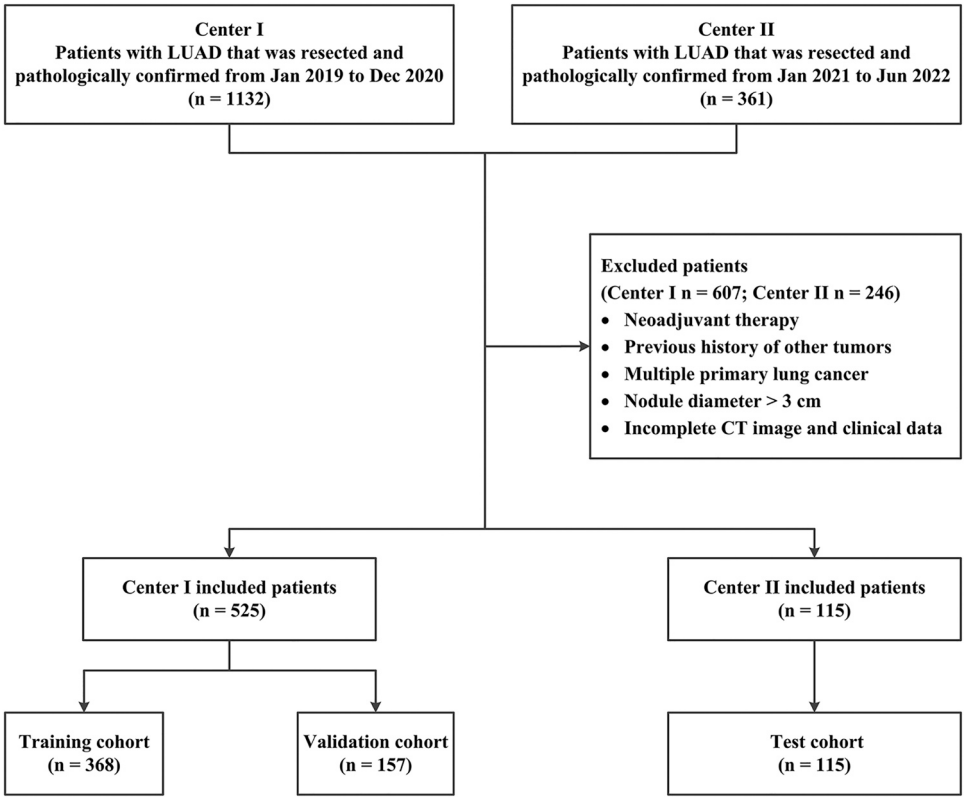


**Fig. 1.** The flowchart for patient's recruitment. LUAD, Lung adenocarcinoma.

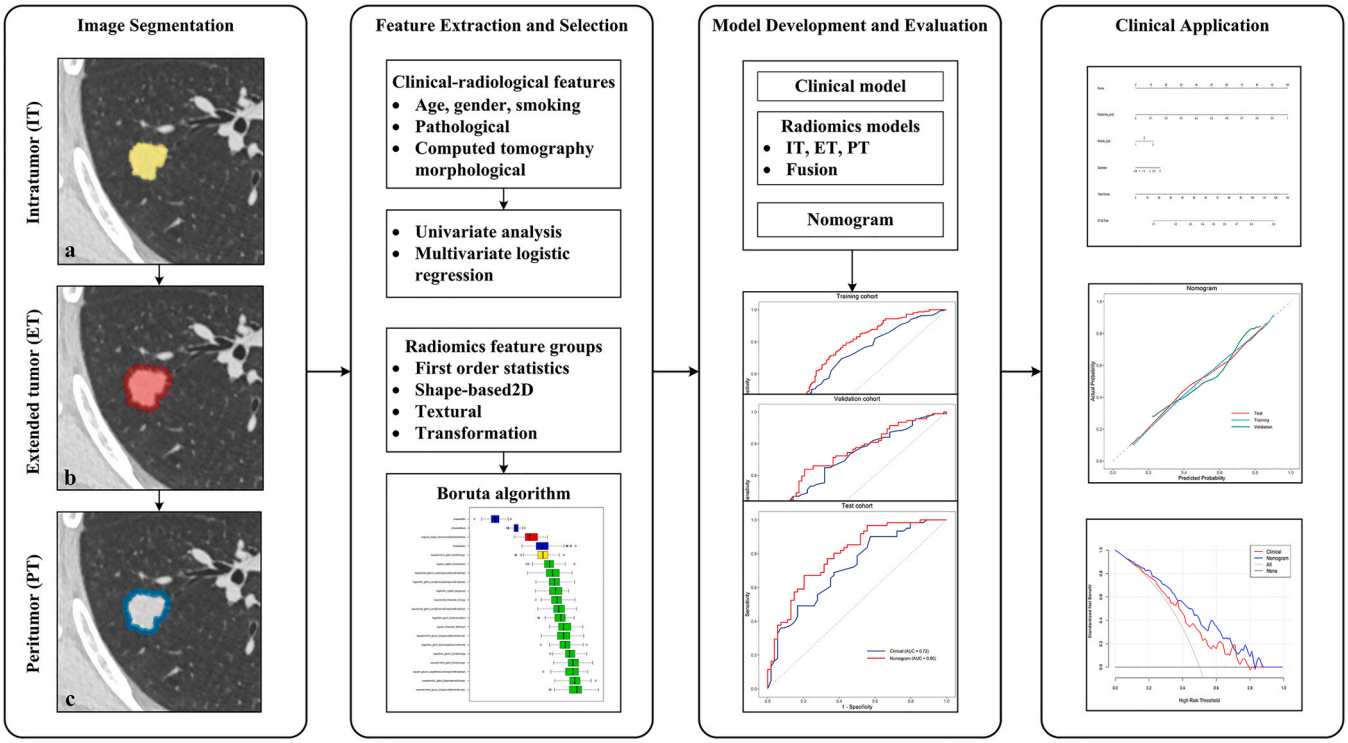


**Fig. 2.** The overall processing workflow. a: Segmenting the tumor edge to obtain the intratumor (IT) ROI. b: Amplifying 5 mm equidistant distance to obtain the extended tumor (ET) ROI. c: Cutting out the acreage of the IT ROI from the ET ROI to get the peritumor (PT) ROI.

the ethics committees of the center I (Number: 2022-KY-E-(106)) and center II (Number: CZLS2022109-A). The requirement for written informed consent was waived. In accordance with the 2021 WHO classification [20], we collected patients with LUAD who accepted surgical resection and confirmed with postoperative pathology. The exclusion criteria were as follows: (i) neoadjuvant therapy (preoperative chemotherapy, radiotherapy, targeted therapy and immunotherapy); (ii) previous history of other tumors; (iii) multiple primary lung cancer; (iv) nodule diameter $> 3$ cm; and (v) incomplete CT image and clinical data. There were two centers in this study, where center I was used to recruit the training and validation cohort (the patients were randomly divided at a ratio of 7:3), and center II was used to recruit the test cohort (Fig. 1).

From medical records, the following clinical and pathological characteristics were collected: age, gender, smoking status (never or smoker), predominant type of adenocarcinoma (lepidic, acinar, papillary, micropapillary or solid), vascular invasion, perineural invasion, pleural invasion, T stage (T1mi, T1a, T1b or T1c) and lymph node metastasis (N0 or N1–3).

### 2.2. CT acquisition and interpretation

CT examinations were performed using nine different scanners from two centers. The specific CT scan parameters are shown in Appendix S1. All images were transmitted to the postprocessing workstation through the Picture Archiving and Communication System for further operation. The lung-window sequences of all cases were reconstructed with the layer thickness ranging from 0.5 to 2.5 mm.

The following CT morphological features were independently assessed by two radiologists: nodule location (right upper lobe, right middle lobe, right lower lobe, left upper lobe or left lower lobe), nodule maximum diameter, nodule type (ground glass, part solid or solid), air bronchogram, vacuole, margin (smooth, lobulated, spiculated, or irregular), pleural indentation and vessel convergence. The consensus was reached by consultation in an event of disagreement. Both radiologists were blinded to the clinical and pathological results.

### 2.3. Histological evaluation

Two pathologists made consistent interpretation of postoperative specimens, and they were blinded to the clinical outcomes. The specimens were fixed with paraformaldehyde, embedded in paraffin and stained with hematoxylin and eosin. The specimen viewing and graphics acquisition instruments were white light photography microscope (Nikon, Eclipse Ci-L) and panoramic section scanner (3DHISTECH, PANNORAMIC DESK/MIDI).

STAS was defined as micropapillary clusters, solid nests, or single cells beyond the edge of the tumor into air spaces in the surrounding lung parenchyma [2]. Micropapillary structures were papillary structures without central fibrovascular cores, and occasionally formed ring-like structures. Solid nests were solid tumor cells clustered into clusters. Single cells were scattered discohesive single cells [5]. The following artifacts should be distinguished from STAS-positive [5,21]: (i) tumor cells with irregular edges and randomly distributed at the edge of the section; (ii) lack of continuum of air spaces containing intra-alveolar tumor cells back to the tumor edge; (iii) alveolar wall cells, bronchial epithelial cells with benign cytological features, or linear strips of cells lifted off of the alveolar walls. The representative pathological images are shown in Fig. S1.

### 2.4. Image segmentation and radiomics features extraction

The image segmentation and radiomics features extraction used a software package called “Radiomics” (Ver1.2.6, syngo.via Frontier, Siemens Healthineers, Forchheim, Germany). We followed the established standards for image segmentation [22]. The overall processing flow is presented in Fig. 2.

(i) The tumor edge was segmented to obtain the intratumor (IT) region of interest (ROI).

(ii) Amplifying 5 mm equidistant distance of the tumor [23] to obtain the extended tumor (ET) ROI.

(iii) Cutting out the acreage of the IT ROI from the ET ROI to obtain

the peritumor (PT) ROI.

One radiologist with 5 years of experience in chest imaging (reader 1) independently segmented the ROI and another radiologist with 25 years of experience in chest imaging (reader 2) examined the ROI. The consensus was reached through consultation in an event of disagreement. After one month later, we selected 50 patients in the training cohort randomly. The reader 1 segmented these cases twice to assess intra-observer reliability. The other radiologist with 10 years of experience in chest imaging (reader 3) segmented the same cases independently to assess inter-observer reliability.

Before feature extraction, all images were resampled to $1 \times 1 \times 1$ mm voxel size by using trilinear interpolation resampling. The extracted radiomics feature groups are shown in Appendix S2.

### 2.5. Radiomics model development

Model development was conducted with R software package (Ver.4.2.6, R Development Core Team: https://www.r-project.org). We used Boruta algorithm to reduce dimensions of the radiomics features and to select important features. The Boruta algorithm is a wrapper build around the random forest classication algorithm, it can calculate each feature's Shapley value and the max shadow value. When a Shapley value was higher than the max shadow value, the truly relevant feature were selected for further analysis [24]. The LinearSVM classifier was used to develop radiomics models. We developed the IT, ET and PT models. Then, we combined the features of IT and PT models to develop the fusion model. Besides, we calculated the prediction probability value for each model.

### 2.6. Nomogram development

The clinical characteristics and CT morphological features with significant differences in the univariate analysis were selected into the multivariate logistic regression to identify clinical independent risk factors of STAS. The nomogram was developed based on the prediction probability value of the optimal radiomics model and clinical independent risk factors.

### 2.7. Statistical analysis

Statistical analysis was conducted in SPSS software (Ver. 26, IBM, Armonk, New York) and the R software package. Two-tailed $p$ value $< 0.05$ indicated a statistically significant difference. The normality of continuous variables was tested using the Kolmogorov−Smirnov test. Differences among normally distributed variables were analyzed with the $t$ test, while non-normal distributed variables were analyzed with the Mann−Whitney $U$ test or Kruskal−Wallis test. Categorical variables were analyzed using the chi-square test or Fisher's precision probability test. Intra-observer and inter-observer reliability were assessed by intraclass correlation coefficients (ICCs). ICC $> 0.80$ indicated good reliability.

The receiver operating characteristic (ROC) curve was plotted, and the area under curve (AUC) was calculated to evaluate the performance of each model. Integrated discrimination improvement (IDI) value was calculated to reflect the improvement of a model performance to another.

The optimal cutoff value for the nomogram scores in the training cohort for predicting STAS status was determined using the Youden index. We used the Hosmer–Lemeshow test and the decision curve analysis (DCA) to evaluate the goodness of fit and clinical application value, respectively.

**Table 1**
Clinical characteristics and CT morphological features of patients in center I.

| Variables | Total (n = 525) | STAS- (n = 218) | STAS+ (n = 307) | $p^a$ | $p^b$ |
|---|---|---|---|---|---|
| Age (y)* | 57 (50−65) | 55 (49−63) | 58 (52−65) | 0.002 | 0.074 |
| Gender | | | | 0.782 | |
| Female | 313 (59.6) | 132 (60.6) | 181 (59.0) | | |
| Male | 212 (40.4) | 86 (39.4) | 126 (41.0) | | |
| Smoking status | | | | 0.079 | |
| Never | 405 (77.1) | 177 (81.2) | 228 (74.3) | | |
| Smoker | 120 (22.9) | 41 (18.8) | 79 (25.7) | | |
| Nodule location | | | | 0.598 | |
| RUL | 185 (35.3) | 77 (35.3) | 108 (35.2) | | |
| RML | 42 (8.0) | 16 (7.4) | 26 (8.5) | | |
| RLL | 91 (17.3) | 36 (16.5) | 55 (17.9) | | |
| LUL | 135 (25.7) | 53 (24.3) | 82 (26.7) | | |
| LLL | 72 (13.7) | 36 (16.5) | 36 (11.7) | | |
| Max diameter (cm)* | 1.8 (1.4–2.2) | 1.6 (1.2–2.0) | 2.0 (1.5–2.3) | < 0.001 | < 0.001 |
| Nodule type | | | | < 0.001 | < 0.001 |
| Ground glass | 57 (10.9) | 39 (17.9) | 18 (5.8) | | Referent |
| Part solid | 266 (50.7) | 127 (58.3) | 139 (45.3) | | 0.117 |
| Solid | 202 (38.4) | 52 (23.9) | 150 (48.9) | | < 0.001 |
| Air bronchogram | | | | 0.602 | |
| Absent | 247 (47.0) | 106 (48.6) | 141 (45.9) | | |
| Present | 278 (53.0) | 112 (51.4) | 166 (54.1) | | |
| Vacuole | | | | 0.516 | |
| Absent | 361 (68.8) | 146 (67.0) | 215 (70.0) | | |
| Present | 164 (31.2) | 72 (33.0) | 92 (30.0) | | |
| Margin | | | | 0.024 | 0.888 |
| Smooth | 80 (15.2) | 43 (19.7) | 37 (12.0) | | Referent |
| Lobulated | 196 (37.4) | 69 (31.7) | 127 (41.4) | | 0.902 |
| Spiculated | 106 (20.2) | 41 (18.8) | 65 (21.2) | | 0.455 |
| Irregular | 143 (27.2) | 65 (29.8) | 78 (25.4) | | 0.801 |
| Pleural indentation | | | | < 0.001 | 0.165 |
| Absent | 191 (36.4) | 102 (46.8) | 89 (29.0) | | |
| Present | 334 (63.6) | 116 (53.2) | 218 (71.0) | | |
| Vessel convergence | | | | 0.332 | |
| Absent | 10 (1.9) | 6 (2.8) | 4 (1.3) | | |
| Present | 515 (98.1) | 212 (97.2) | 303 (98.7) | | |

Note. STAS, Spread through air spaces; RUL, Right upper lobe; RML, Right middle lobe; RLL, Right lower lobe; LUL, Left upper lobe; LLL, Left lower lobe.
[a]: Univariate analysis
[b]: Multivariate analysis
*: Data are the median, and data in parentheses are the interquartile range.

## 3. Results

### 3.1. Baseline characteristics

In center I, 525 patients with pathologically confirmed LUAD were included. Among these patients, there were 307 (58.5 %) patients with and 218 (41.5 %) patients without STAS. The clinical characteristics and CT morphological features of the patients are summarized in Table 1. The pathological characteristics are summarized in Table S1.

Most clinical characteristics and CT morphological features showed no significant differences between the training, validation and test cohorts. Therefore, the data was suitable for developing and validating models in different centers (Table S2).

### 3.2. Development and evaluation of the clinical model

In the univariate analysis, age, maximum diameter, nodule type, margin, pleural indentation, predominant type, vascular invasion, pleural invasion, T stage and lymph node metastasis showed significant differences between STAS-positive and STAS-negative patients. In the

**Table 2**
Prediction performance of all models.

| Cohort | Model | AUC (95 %CI ) | Sensitivity | Specificity | Accuracy | PPV | NPV | F1 |
|---|---|---|---|---|---|---|---|---|
| Training | Clinical | 0.68 (0.63, 0.74) | 0.69 | 0.59 | 0.65 | 0.70 | 0.58 | 0.70 |
| | Intratumor | 0.72 (0.67, 0.76) | 0.69 | 0.66 | 0.68 | 0.74 | 0.61 | 0.71 |
| | Extended tumor | 0.74 (0.68, 0.79) | 0.76 | 0.63 | 0.70 | 0.74 | 0.65 | 0.75 |
| | Peritumor | 0.71 (0.66, 0.77) | 0.70 | 0.65 | 0.68 | 0.73 | 0.61 | 0.72 |
| | Fusion | 0.73 (0.68, 0.78) | 0.72 | 0.64 | 0.69 | 0.74 | 0.63 | 0.73 |
| | Nomogram | 0.73 (0.68, 0.79) | 0.70 | 0.66 | 0.69 | 0.80 | 0.54 | 0.75 |
| Validation | Clinical | 0.69 (0.61, 0.78) | 0.66 | 0.63 | 0.65 | 0.73 | 0.56 | 0.69 |
| | Intratumor | 0.70 (0.61, 0.78) | 0.60 | 0.71 | 0.64 | 0.76 | 0.54 | 0.67 |
| | Extended tumor | 0.71 (0.62, 0.79) | 0.73 | 0.67 | 0.71 | 0.77 | 0.63 | 0.75 |
| | Peritumor | 0.73 (0.65, 0.84) | 0.67 | 0.67 | 0.67 | 0.75 | 0.58 | 0.71 |
| | Fusion | 0.72 (0.64, 0.80) | 0.65 | 0.71 | 0.68 | 0.77 | 0.58 | 0.71 |
| | Nomogram | 0.72 (0.64, 0.80) | 0.68 | 0.60 | 0.66 | 0.81 | 0.43 | 0.74 |
| Test | Clinical | 0.72 (0.62, 0.81) | 0.72 | 0.52 | 0.63 | 0.63 | 0.62 | 0.67 |
| | Intratumor | 0.70 (0.60, 0.80) | 0.66 | 0.61 | 0.63 | 0.66 | 0.61 | 0.66 |
| | Extended tumor | 0.80 (0.72, 0.88) | 0.80 | 0.59 | 0.70 | 0.69 | 0.73 | 0.74 |
| | Peritumor | 0.75 (0.68, 0.78) | 0.75 | 0.61 | 0.69 | 0.69 | 0.69 | 0.72 |
| | Fusion | 0.73 (0.64, 0.72) | 0.77 | 0.63 | 0.70 | 0.70 | 0.70 | 0.73 |
| | Nomogram | 0.80 (0.72, 0.88) | 0.70 | 0.71 | 0.70 | 0.77 | 0.63 | 0.73 |

Note. AUC, Area under curve; CI, Confidence interval; PPV, Positive predictive value; NPV, Negative predictive value.

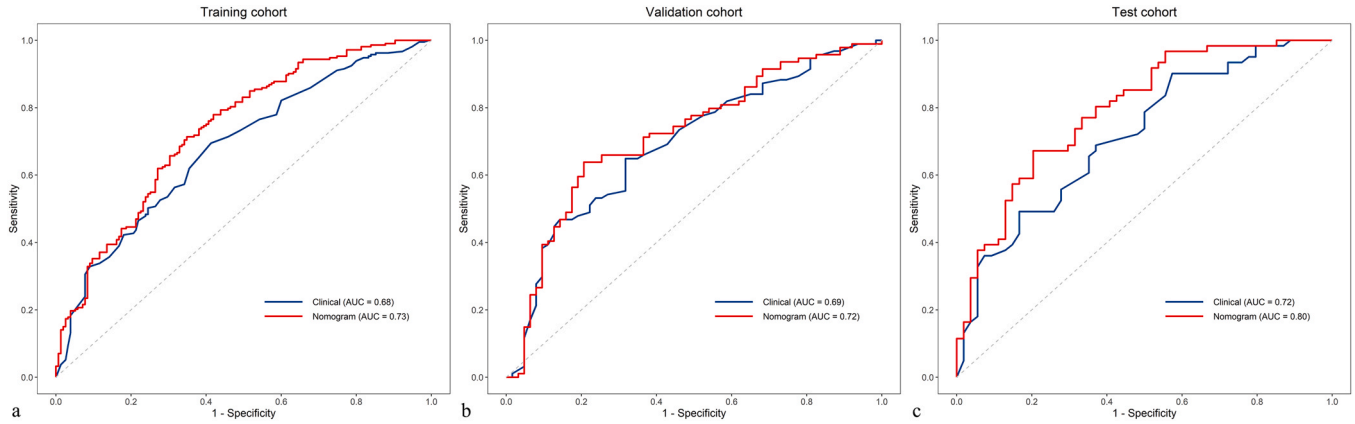


**Fig. 3.** Receiver operating characteristic curves of the nomogram and the clinical model. a/b/c: receiver operating characteristic curves of two models in the training, validation and test cohort, respectively. AUC, Area under curve.

**Table 3**
Performance improvement of models.

| Model | NRI | | IDI | |
|---|---|---|---|---|
| | Statistics (95 % CI) | *p* | Statistics (95 % CI) | *p* |
| Peritumor vs Intratumor | 0.16 (0, 0.33) | 0.050 | 0.05 (0, 0.09) | 0.040 |
| Extended tumor vs Intratumor | 0.43 (0.23, 0.62) | < 0.001 | 0.14 (0.08, 0.20) | < 0.001 |
| Extended tumor vs Peritumor | 0.24 (0.05, 0.44) | 0.010 | 0.09 (0.03, 0.15) | 0.004 |
| Extended tumor vs Fusion | 0.31 (0.11, 0.50) | 0.002 | 0.11 (0.05, 0.16) | < 0.001 |
| Fusion vs Intratumor | 0.12 (0.01, 0.23) | 0.040 | 0.03 (0.11, 0.50) | < 0.001 |
| Fusion vs Peritumor | −0.04 (−0.17, 0.08) | 0.470 | −0.02 (−0.05, 0.01) | 0.300 |
| Nomogram vs Clinical | 0.43 (0.23, 0.64) | < 0.001 | 0.12 (0.06, 0.19) | < 0.001 |

Note. CI, Confidence interval; IDI, Integrated discrimination improvement; NRI, Net reclassification index.

multivariate logistic regression, maximum diameter ($p < 0.001$) and nodule type ($p < 0.001$) were clinical independent risk factors of STAS.

Clinical independent risk factors were used to develop the clinical model. The AUC value was 0.68, 0.69 and 0.72 in the training, validation and test cohorts, respectively (Table 2 and Fig. 3).

### 3.3. Development and evaluation of radiomics models

We extracted 1226 radiomics features from each ROI, respectively. The intra-observer ICCs ranged from 0.89 to 0.97. The inter-observer ICCs ranged from 0.83 to 0.90. After dimensionality reduction by boruta algorithm, 10, 15 and 9 features were selected to develop the IT, ET and PT model, respectively (Table S3 and Fig. S2).

In the training, validation and test cohorts, the ET model achieved an AUC of 0.74, 0.71 and 0.80, respectively, which was higher compared with the IT model (AUC of 0.72, 0.70 and 0.70) and the PT model (AUC of 0.71, 0.73 and 0.75). The fusion model based on the features of IT and PT models had an AUC of 0.73, 0.72 and 0.73 (Table 2). The ET model performed better than other radiomics models with the IDI value increased $\geq 9$ % ($p < 0.05$) (Table 3).

### 3.4. Clinical application

The prediction probability value of the ET model, maximum diameter and nodule type were entered into the nomogram. Fig. 3 shows ROC curves of the clinical model and nomogram. The nomogram outperformed compared to the clinical model with the IDI value of 12 % ($p < 0.001$) (Table 3). The plot of the nomogram is shown in Fig. 4.

The optimal cutoff value for predicting STAS status by the nomogram

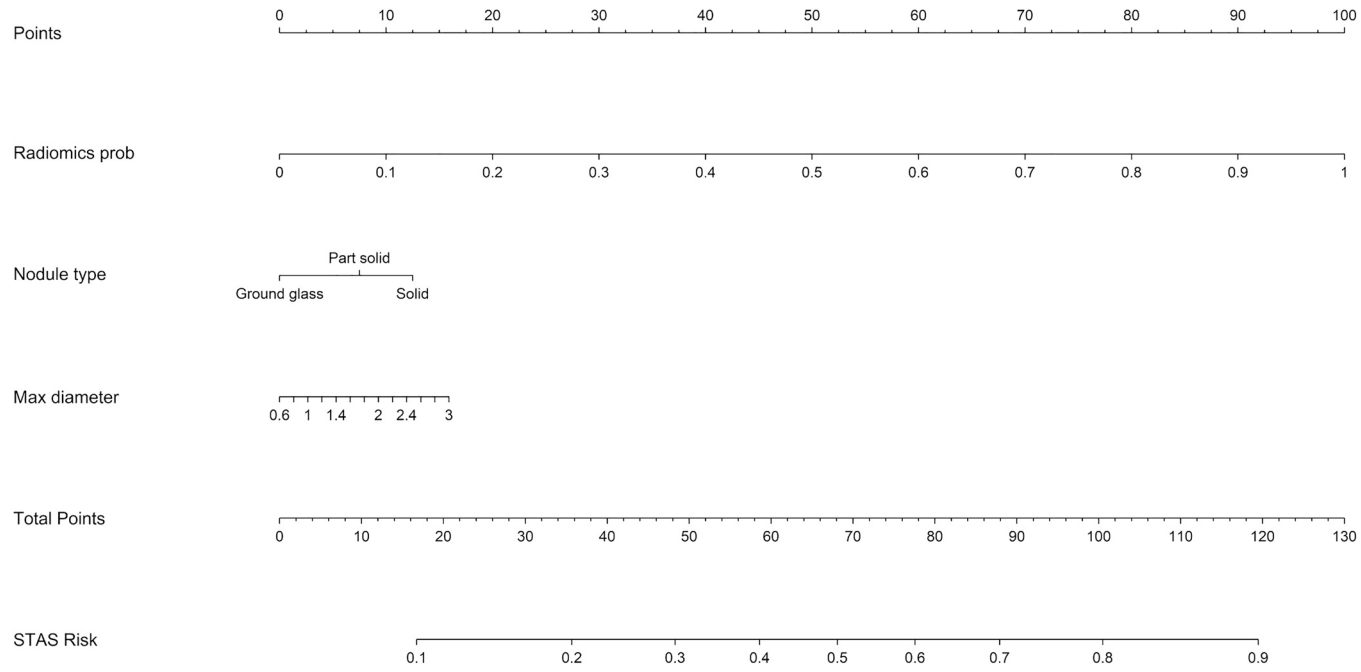


**Fig. 4.** The nomogram based on the prediction probability value of the extended tumor model, maximum tumor diameter and nodule type. Radiomics prob, prediction probability value of the extended tumor model.

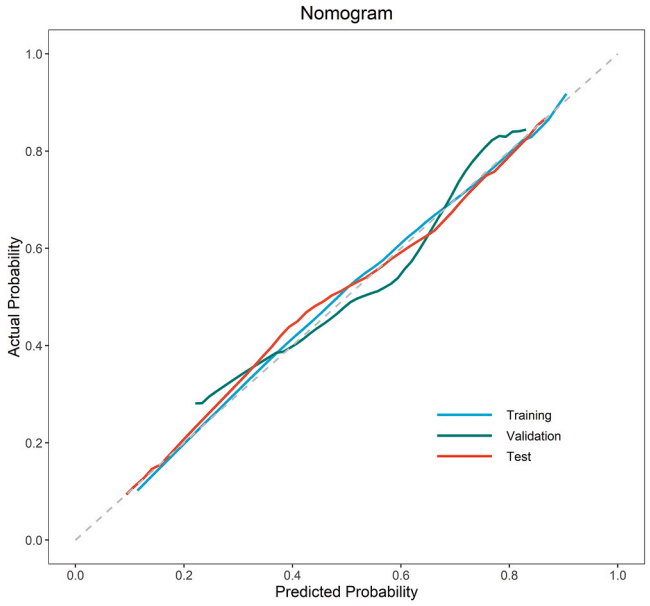


**Fig. 5.** Calibration curves of the nomogram in the training, validation and test cohorts.

score was 77.31. When the nomogram score is equal to or greater than 77.31, patients will be identified as STAS-positive. The Hosmer–Lemeshow test showed that the nomogram fitted well in the training, validation and test cohorts ($p > 0.05$) (Fig. 5). Between the DCA curves, when the threshold probability was about 0.1–0.9, the nomogram obtained a better clinical net benefit and diagnostic value compared with the clinical model (Fig. 6).

## 4. Discussion

This multicenter study attempted to explore the value of intratumoral and peritumoral information in predicting STAS status and provide decision support for surgery planning in LUAD with diameter $\leq 3$ cm. The results showed that the PT model performed better than the IT model. The ET model outperformed other radiomics models. The nomogram performed better than the clinical model and it had good clinical application value in the prediction of STAS status.

In our study, the maximum diameter and nodule type were independent risk factor for STAS, and these results are basically consistent with other studies [9,10,25–28]. A larger tumor diameter, is associated with a higher STAS-positive rate, which might be related to the T stage that reflects the invasiveness of the tumor [29]. Our study revealed that STAS status significantly correlated with predominant type. Among these subtypes, micropapillary and solid pattern was prevalent in STAS-positive patients, whereas lepidic pattern was more common in STAS-negative patients. Some previous studies [30–32] are consistent with our results. Zhang et al. [33] reported that different LUAD predominant types revealed disparate nodule types on CT image, which might partially explain the reason for the association between STAS and nodule type.

We segmented the IT, ET and PT ROIs to developed radiomics models. Our results showed that the PT model had higher predictive value than the IT model. The reason might be related to the distribution of STAS. STAS is scattered in the peritumoral lung parenchyma, so intratumoral features may only indirectly predict STAS status and peritumoral information could offer a better prediction of STAS status, which is consistent with the pathological distribution. Liao et al. [19] segmented the ROI with equidistant amplification and found the same result. The ET model performed better than the IT and PT models. The possible reason might be that the ET ROI not only has the actual spatial information of STAS, but also includes intratumoral information, which is highly related to tumor invasiveness [34].

In our study, we developed the fusion model by combining the features of IT and PT models. The fusion model underperformed compared to the ET model, which could be due to the presence of redundancy when integrating two models with different ROIs, thus causing a negative impact on the performance [35]. Therefore, when in the same acreage of the region, the radiomics features extracted from the whole region directly will perform better than integrating the features extracted from each part region.

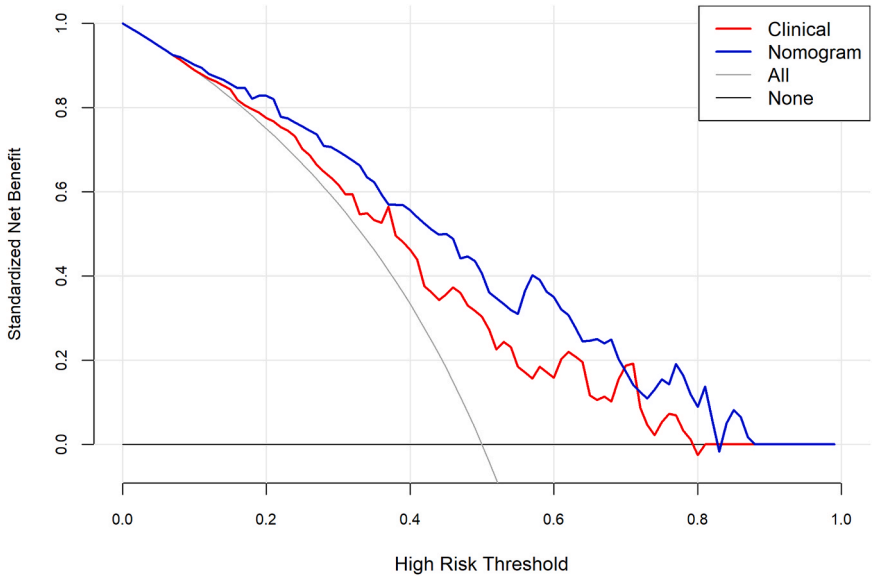


**Fig. 6.** Decision curve analysis curves of the nomogram and the clinical model. It showed when the threshold probability was about 0.1–0.9, the nomogram obtained better clinical net benefit compared with the clinical model.

The mining of radiomics biomarkers is almost completely driven by data, and there may be collinearity among radiomics features in the model, so the poor biological interpretability of radiomics features would lead to clinical application obstacles [36]. To solve this problem, we developed the nomogram combined by the prediction probability value of the ET model and clinical independent risk factors, and we calculated the optimal cutoff value for the nomogram score to identified STAS status. The nomogram performed significantly better than the clinical model, and had important value in risk stratification of STAS status. In a previous study, Jiang et al. [14] developed a model to predict STAS status based on tumor radiomics features and clinical data and obtained a poorer performance than our result. This might be because some important CT morphological features such as nodule diameter and nodule type were not included into their model. In another study [37], the AUC value of the nomogram in test cohort got as high as 0.99, however the calibration curve performed poorly. This could be because, when segmenting the ROI, spherical amplification not only lost information about the effective region, but also included redundant information. Furthermore, their sample capacity was not big enough to reflect authenticity of the data.

There were several limitations to this study. First, this was a retrospective study, which may have led to potential selection bias, and our results need to be further verified in prospective research. Second, this was a conventional radiomics study which depends on manual segmentation. Deep learning can automatically learn which features are best for a task, and will be using in our future study. Third, follow-up data were not collected due to insufficient period, and we will continue to collect long-term follow-up data and assess the impact of STAS for patient prognosis in the future. Fourth, although the nomogram can visually calculate the risk of prediction result, conveying these concepts to patients is challenging, and we need design more simple-to-used method such as interactive website in the future.

In conclusion, peritumoral information is significant to predict STAS status. The nomogram based on the prediction probability value of the ET model and clinical independent risk factors can predict the STAS status in LUAD with diameter $\leq 3$ cm. When the nomogram score $\geq 77.31$, the patients will be identified as STAS-positive, which can provide decision support for surgery planning. Future studies should adopt deep learning models to automatically acquire features related to the STAS status of LUAD, avoiding the bias caused by manual segmentation of traditional radiomics. In addition, further follow-up data should be collected to assess the impact of STAS on patient outcomes in the future.

## Funding

This study has received funding by the Chongqing Key Medical Research Project of Combination of Science and Medicine (No. 2023ZDXM010), the Natural Science Foundation of Chongqing municipality (No. CSTB2022NSCQ-MSX1286), the Chongqing Medical Research Project of Combination of Science and Medicine (No. 2023MSXM038), the Scientific and Technological Research Program of Chongqing Municipal Education Commission (No. KJQN202300128), the Chongqing Medical Research Project of Combination of Science and Medicine (No. 2025MSXM032), the National Natural Science Foundation of China (No. 82402257) and the Guangxi Medical and Health Appropriate Technology Development and Application Project (No. S2020036).

## Ethical statement

The study was conducted in accordance with the Declaration of Helsinki (as revised in 2013). This retrospective study was approved by the ethics committees of The First Affiliated Hospital of Guangxi Medical University (Number: 2022-KY-E-(106)) and Chongqing University Cancer Hospital (Number: CZLS2022109-A). The individual consent for this analysis was waived.

## CRediT authorship contribution statement

**Lihua Chen:** Writing – review & editing, Supervision, Methodology, Funding acquisition, Conceptualization. **Kai Li:** Validation, Resources, Methodology, Funding acquisition, Conceptualization. **Changyu Liang:** Investigation. **Xiaosong Lan:** Visualization, Software, Formal analysis, Data curation. **Jiuquan Zhang:** Resources, Project administration, Funding acquisition. **Xuemei Huang:** Investigation. **Junli Tao:** Writing – review & editing, Methodology, Funding acquisition, Conceptualization. **Yangfan Su:** Writing – original draft, Visualization, Methodology, Formal analysis, Conceptualization.

## Declaration of Competing Interest

The authors declare that they have no known competing financial interests or personal relationships that could have appeared to influence the work reported in this paper.

## Acknowledgments

We thank the study participants and referring technicians for their participation in this study. This study has received funding by the Chongqing Key Medical Research Project of Combination of Science and Medicine (No. 2023ZDXM010), the Natural Science Foundation of Chongqing municipality (No. CSTB2022NSCQ-MSX1286), the Chongqing Medical Research Project of Combination of Science and Medicine (No. 2023MSXM038), the Scientific and Technological Research Program of Chongqing Municipal Education Commission (No. KJQN202300128), the Chongqing Medical Research Project of Combination of Science and Medicine (No. 2025MSXM032), the National Natural Science Foundation of China (No. 82402257) and the Guangxi Medical and Health Appropriate Technology Development and Application Project (No. S2020036).

## Appendix A. Supporting information

Supplementary data associated with this article can be found in the online version at doi:10.1016/j.ejro.2024.100630.

## References

[1] R.L. Siegel, K.D. Miller, N.S. Wagle, A. Jemal, Cancer statistics, 2023, CA: A Cancer J. Clin. 73 (1) (2023) 17–48.
[2] W.D. Travis, E. Brambilla, A.G. Nicholson, Y. Yatabe, J.H.M. Austin, M.B. Beasley, L.R. Chirieac, S. Dacic, E. Duhig, D.B. Flieder, K. Geisinger, F.R. Hirsch, Y. Ishikawa, K.M. Kerr, M. Noguchi, G. Pelosi, C.A. Powell, M.S. Tsao, I. Wistuba, W.H.O. Panel, The 2015 World Health Organization Classification of Lung Tumors: impact of genetic, clinical and radiologic advances since the 2004 classification, J. Thorac. Oncol. 10 (9) (2015) 1243–1260.
[3] H. Ito, K. Suzuki, T. Mizutani, K. Aokage, M. Wakabayashi, H. Fukuda, S.-i Watanabe, H. Ito, K. Suzuki, T. Mizutani, K. Aokage, M. Wakabayashi, T. Koike, Y. Tsutani, H. Saji, K. Nakagawa, Y. Zenke, K. Takamochi, T. Aoki, J. Okami, H. Yoshioka, S. Shiono, M. Okada, S.-i Watanabe, Long-term survival outcome after lobectomy in patients with clinical T1 N0 lung cancer, J. Thorac. Cardiovasc. Surg. 161 (1) (2021) 281–290.
[4] K. Aokage, K. Suzuki, H. Saji, M. Wakabayashi, T. Kataoka, Y. Sekino, H. Fukuda, M. Endo, A. Hattori, T. Mimae, T. Miyoshi, M. Isaka, H. Yoshioka, R. Nakajima, K. Nakagawa, J. Okami, H. Ito, H. Kuroda, M. Tsuboi, N. Okumura, M. Takahama, Y. Ohde, T. Aoki, Y. Tsutani, M. Okada, S.I. Watanabe, G. Japan Clinical Oncology, Segmentectomy for ground-glass-dominant lung cancer with a tumour diameter of 3 cm or less including ground-glass opacity (JCOG1211): a multicentre, single-arm, confirmatory, phase 3 trial, Lancet Respir. Med 11 (6) (2023) 540–549.
[5] K. Kadota, J.I. Nitadori, C.S. Sima, H. Ujiie, N.P. Rizk, D.R. Jones, P.S. Adusumilli, W.D. Travis, Tumor spread through air spaces is an important pattern of invasion and impacts the frequency and location of recurrences after limited resection for small stage I lung adenocarcinomas, J. Thorac. Oncol. 10 (5) (2015) 806–814.
[6] T. Eguchi, K. Kameda, S. Lu, M.J. Bott, K.S. Tan, J. Montecalvo, J.C. Chang, N. Rekhtman, D.R. Jones, W.D. Travis, P.S. Adusumilli, Lobectomy is associated with better outcomes than sublobar resection in spread through air spaces (STAS)-positive T1 lung adenocarcinoma: a propensity score-matched analysis, J. Thorac. Oncol. 14 (1) (2019) 87–98.
[7] M.A. Medina, A.M. Onken, C. de Margerie-Mellon, B.H. Heidinger, Y. Chen, A. A. Bankier, P.A. VanderLaan, Preoperative bronchial cytology for the assessment of tumor spread through air spaces in lung adenocarcinoma resection specimens, Cancer Cytopathol. 128 (4) (2020) 278–286.
[8] F. Zhou, J.A. Villalba, T.M.S. Sayo, N. Narula, H. Pass, M. Mino-Kenudson, A. L. Moreira, Assessment of the feasibility of frozen sections for the detection of spread through air spaces (STAS) in pulmonary adenocarcinoma, Mod. Pathol. 35 (2) (2022) 210–217.
[9] S.K. Kim, T.J. Kim, M.J. Chung, T.S. Kim, K.S. Lee, J.I. Zo, Y.M. Shim, Lung Adenocarcinoma: CT features associated with spread through air spaces, Radiology 289 (3) (2018) 831–840.
[10] G. Toyokawa, Y. Yamada, T. Tagawa, T. Kamitani, Y. Yamasaki, M. Shimokawa, Y. Oda, Y. Maehara, Computed tomography features of resected lung adenocarcinomas with spread through air spaces, J. Thorac. Cardiovasc. Surg. 156 (4) (2018) 1670–1676.e4.
[11] R.J. Gillies, P.E. Kinahan, H. Hricak, Radiomics: images are more than pictures, they are data, Radiology 278 (2) (2016) 563–577.
[12] J. Tao, C. Liang, K. Yin, J. Fang, B. Chen, Z. Wang, X. Lan, J. Zhang, 3D convolutional neural network model from contrast-enhanced CT to predict spread through air spaces in non-small cell lung cancer, Diagn. Interv. Imaging 103 (11) (2022) 535–544.
[13] Y. Onozato, T. Nakajima, H. Yokota, J. Morimoto, A. Nishiyama, T. Toyoda, T. Inage, K. Tanaka, Y. Sakairi, H. Suzuki, T. Uno, I. Yoshino, Radiomics is feasible for prediction of spread through air spaces in patients with nonsmall cell lung cancer, Sci. Rep. 11 (1) (2021) 13526.
[14] C. Jiang, Y. Luo, J. Yuan, S. You, Z. Chen, M. Wu, G. Wang, J. Gong, CT-based radiomics and machine learning to predict spread through air space in lung adenocarcinoma, Eur. Radio. 30 (7) (2020) 4050–4057.
[15] D. Chen, Y. She, T. Wang, H. Xie, J. Li, G. Jiang, Y. Chen, L. Zhang, D. Xie, C. Chen, Radiomics-based prediction for tumour spread through air spaces in stage I lung adenocarcinoma using machine learning, Eur. J. Cardiothorac. Surg. 58 (1) (2020) 51–58.
[16] Y. Wang, D. Lyu, L. Hu, J. Wu, S. Duan, T. Zhou, W. Tu, Y. Xiao, L. Fan, S. Liu, CT-based intratumoral and peritumoral radiomics nomograms for the preoperative prediction of spread through air spaces in clinical stage IA non-small cell lung cancer, J. Imaging Inform. Med. 37 (2) (2024) 520–535.
[17] L. Qi, X. Li, L. He, G. Cheng, Y. Cai, K. Xue, M. Li, Comparison of diagnostic performance of spread through airspaces of lung adenocarcinoma based on morphological analysis and perinodular and intranodular radiomic features on chest CT images, Front Oncol. 11 (2021) 654413.
[18] K. Takehana, R. Sakamoto, K. Fujimoto, Y. Matsuo, N. Nakajima, A. Yoshizawa, T. Menju, M. Nakamura, R. Yamada, T. Mizowaki, Y. Nakamoto, Peritumoral radiomics features on preoperative thin-slice CT images can predict the spread through air spaces of lung adenocarcinoma, Sci. Rep. 12 (1) (2022) 10323.
[19] G. Liao, L. Huang, S. Wu, P. Zhang, D. Xie, L. Yao, Z. Zhang, S. Yao, L. Shanshan, S. Wang, G. Wang, L. Wing-Chi Chan, H. Zhou, Preoperative CT-based peritumoral and tumoral radiomic features prediction for tumor spread through air spaces in clinical stage I lung adenocarcinoma, Lung Cancer 163 (2022) 87–95.
[20] A.G. Nicholson, M.S. Tsao, M.B. Beasley, A.C. Borczuk, E. Brambilla, W.A. Cooper, S. Dacic, D. Jain, K.M. Kerr, S. Lantuejoul, M. Noguchi, M. Papotti, N. Rekhtman, G. Scagliotti, P. van Schil, L. Sholl, Y. Yatabe, A. Yoshida, W.D. Travis, The 2021 WHO classification of lung tumors: impact of advances since 2015, J. Thorac. Oncol. 17 (3) (2022) 362–387.
[21] R.G. Aly, N. Rekhtman, X. Li, Y. Takahashi, T. Eguchi, K.S. Tan, C.M. Rudin, P. S. Adusumilli, W.D. Travis, Spread through air spaces (STAS) is prognostic in atypical carcinoid, large cell neuroendocrine carcinoma, and small cell carcinoma of the lung, J. Thorac. Oncol. 14 (9) (2019) 1583–1593.
[22] A.A. Bankier, H. MacMahon, J.M. Goo, G.D. Rubin, C.M. Schaefer-Prokop, D. P. Naidich, Recommendations for measuring pulmonary nodules at CT: a statement from the fleischner society, Radiology 285 (2) (2017) 584–600.
[23] N. Beig, M. Khorrami, M. Alilou, P. Prasanna, N. Braman, M. Orooji, S. Rakshit, K. Bera, P. Rajiah, J. Ginsberg, C. Donatelli, R. Thawani, M. Yang, F. Jacono, P. Tiwari, V. Velcheti, R. Gilkeson, P. Linden, A. Madabhushi, Perinodular and intranodular radiomic features on lung CT images distinguish Adenocarcinomas from Granulomas, Radiology 290 (3) (2019) 783–792.
[24] M.B. Kursa, W.R. Rudnicki, Feature selection with the Boruta package, J. Stat. Softw. 36 (11) (2010) 1–13.
[25] C. de Margerie-Mellon, A. Onken, B.H. Heidinger, P.A. VanderLaan, A.A. Bankier, CT Manifestations of tumor spread through airspaces in pulmonary adenocarcinomas presenting as subsolid nodules, J. Thorac. Imaging 33 (6) (2018) 402–408.
[26] S. Koezuka, T. Mikami, N. Tochigi, A. Sano, Y. Azuma, T. Makino, H. Otsuka, K. Matsumoto, N. Shiraga, A. Iyoda, Toward improving prognosis prediction in patients undergoing small lung adenocarcinoma resection: radiological and pathological assessment of diversity and intratumor heterogeneity, Lung Cancer 135 (2019) 40–46.
[27] Y. Chen, C. Jiang, W. Kang, J. Gong, D. Luo, S. You, Z. Cheng, Y. Luo, K. Wu, Development and validation of a CT-based nomogram to predict spread through air space (STAS) in peripheral stage IA lung adenocarcinoma, Jpn J. Radio. 40 (6) (2022) 586–594.
[28] S. Shiono, N. Yanagawa, Spread through air spaces is a predictive factor of recurrence and a prognostic factor in stage I lung adenocarcinoma, Inter. Cardiovasc Thorac. Surg. 23 (4) (2016) 567–572.
[29] B.W. Carter, J.P. Lichtenberger, M.K. Benveniste, P.M. de Groot, C.C. Wu, J. J. Erasmus, M.T. Truong, Revisions to the TNM staging of lung cancer: rationale, significance, and clinical application, RadioGraphics 38 (2) (2018) 374–391.
[30] L. Cao, M. Jia, P.L. Sun, H. Gao, Histopathologic features from preoperative biopsies to predict spread through air spaces in early-stage lung adenocarcinoma: a retrospective study, BMC Cancer 21 (1) (2021) 913.
[31] Y.B. Han, H. Kim, M. Mino-Kenudson, S. Cho, H.J. Kwon, K.R. Lee, S. Kwon, J. Lee, K. Kim, S. Jheon, C.T. Lee, J.S. Lee, W. Kook, J.H. Chung, Tumor spread through air spaces (STAS): prognostic significance of grading in non-small cell lung cancer, Mod. Pathol. 34 (3) (2021) 549–561.
[32] C. Dai, H. Xie, H. Su, Y. She, E. Zhu, Z. Fan, F. Zhou, Y. Ren, D. Xie, H. Zheng, X. Kadeer, D. Chen, L. Zhang, G. Jiang, C. Wu, C. Chen, Tumor spread through air spaces affects the recurrence and overall survival in patients with lung Adenocarcinoma > 2 to 3 cm, J. Thorac. Oncol. 12 (7) (2017) 1052–1060.
[33] Y. Zhang, F. Fu, H. Chen, Management of ground-glass opacities in the lung cancer spectrum, Ann. Thorac. Surg. 110 (6) (2020) 1796–1804.
[34] Q. Chen, J. Shao, T. Xue, H. Peng, M. Li, S. Duan, F. Feng, Intratumoral and peritumoral radiomics nomograms for the preoperative prediction of lymphovascular invasion and overall survival in non-small cell lung cancer, Eur. Radiol. 33 (2) (2022) 947–958.

[35] N. Timme, W. Alford, B. Flecker, J.M. Beggs, Synergy, redundancy, and multivariate information measures: an experimentalist's perspective, J. Comput. Neurosci. 36 (2) (2013) 119–140.
[36] W.L. Bi, A. Hosny, M.B. Schabath, M.L. Giger, N.J. Birkbak, A. Mehrtash, T. Allison, O. Arnaout, C. Abbosh, I.F. Dunn, R.H. Mak, R.M. Tamimi, C.M. Tempany, C. Swanton, U. Hoffmann, L.H. Schwartz, R.J. Gillies, R.Y. Huang, H. Aerts, Artificial intelligence in cancer imaging: clinical challenges and applications, CA Cancer J. Clin. 69 (2) (2019) 127–157.
[37] Y. Zhuo, M. Feng, S. Yang, L. Zhou, D. Ge, S. Lu, L. Liu, F. Shan, Z. Zhang, Radiomics nomograms of tumors and peritumoral regions for the preoperative prediction of spread through air spaces in lung adenocarcinoma, Transl. Oncol. 13 (10) (2020) 100820.